

# Precise Prediction for the Mass of the Lightest Higgs Boson in the MSSM

S. HEINEMEYER, W. HOLLIK AND G. WEIGLEIN

*Institut für Theoretische Physik, Universität Karlsruhe,  
D-76128 Karlsruhe, Germany*

## Abstract

The leading diagrammatic two-loop corrections are incorporated into the prediction for the mass of the lightest Higgs boson,  $m_h$ , in the Minimal Supersymmetric Standard Model (MSSM). The results, containing the complete diagrammatic one-loop corrections, the new two-loop result and refinement terms incorporating leading electroweak two-loop and higher-order QCD contributions, are discussed and compared with results obtained by renormalization group calculations. Good agreement is found in the case of vanishing mixing in the scalar quark sector, while sizable deviations occur if squark mixing is taken into account.

The search for the lightest Higgs boson provides a direct and very stringent test of Supersymmetry (SUSY), since the prediction of a relatively light Higgs boson is common to all Supersymmetric models whose couplings remain in the perturbative regime up to a very high energy scale [1]. A precise prediction for the mass of the lightest Higgs boson in terms of the relevant SUSY parameters is crucial in order to determine the discovery and exclusion potential of LEP2 and the upgraded Tevatron and also for physics at the LHC, where eventually a high-precision measurement of the mass of this particle might be possible.

In the Minimal Supersymmetric Standard Model (MSSM) [2] the mass of the lightest Higgs boson,  $m_h$ , is restricted at the tree level to be smaller than the  $Z$ -boson mass. This bound, however, is strongly affected by the inclusion of radiative corrections. The dominant one-loop corrections arise from the top and scalar-top sector via terms of the form  $G_F m_t^4 \ln(m_{\tilde{t}_1} m_{\tilde{t}_2} / m_t^2)$  [3]. They increase the predicted values of  $m_h$  and yield an upper bound of about 150 GeV. These results have been improved by performing a complete one-loop calculation in the on-shell scheme, which takes into account the contributions of all sectors of the MSSM [4, 5, 6]. Beyond one-loop order renormalization group (RG) methods have been applied in order to obtain leading logarithmic higher-order contributions [7, 8, 9, 10], and a diagrammatic calculation of the dominant two-loop contributions in the limiting case of vanishing  $\tilde{t}$ -mixing and infinitely large  $M_A$  and  $\tan\beta$  has been carried out [11].

The results of the latter calculations were found to yield considerably lower values for  $m_h$  than the one-loop on-shell calculation. The results obtained within the RG approach differ by up to 20 GeV from the one-loop on-shell result. The bulk of this difference can be attributed to the higher-order leading logarithmic contributions which are included in the RG results. The one-loop result on the other hand contains non-leading contributions which are not included in the RG results and whose size has not yet been precisely determined. Due to the large difference between the complete one-loop on-shell calculation and the RG results, and due to the difficulty in comparing the results of the two approaches, it is not easy to give an estimate for the accuracy of the current theoretical prediction for  $m_h$  in a similar way as done, for instance, for the electroweak precision observables within the Standard Model (SM) (see Ref. [12]).

Recently a Feynman-diagrammatic calculation of the leading two-loop corrections of  $\mathcal{O}(\alpha\alpha_s)$  to the masses of the neutral  $\mathcal{CP}$ -even Higgs bosons has been performed [13]. Compared to the leading one-loop result the two-loop contribution was found to give rise to a considerable reduction of the  $m_h$  value.

It is the purpose of this letter to combine the full diagrammatic one-loop on-shell result [5] with the leading diagrammatic two-loop result [13], and to obtain in this way the currently most precise prediction for  $m_h$  within the Feynman-diagrammatic approach for arbitrary values of the parameters of the Higgs and scalar top sector of the MSSM. Further refinements concerning the leading two-loop Yukawa corrections of  $\mathcal{O}(G_F^2 m_t^6)$  [8, 14] and of leading QCD corrections beyond two-loop order are included. The resulting predictions for  $m_h$  are discussed in view of the discovery potential of LEP2 [15] and are compared with the results obtained using the RG approach [8, 9, 10].

Contrary to the SM, in the MSSM two Higgs doublets are needed. The Higgs potential

is given by [16]

$$V = m_1^2 H_1 \bar{H}_1 + m_2^2 H_2 \bar{H}_2 - m_{12}^2 (\epsilon_{ab} H_1^a H_2^b + \text{h.c.}) + \frac{g'^2 + g^2}{8} (H_1 \bar{H}_1 - H_2 \bar{H}_2)^2 + \frac{g^2}{2} |H_1 \bar{H}_2|^2, \quad (1)$$

where  $m_1, m_2, m_{12}$  are soft SUSY-breaking terms,  $g, g'$  are the  $SU(2)$  and  $U(1)$  gauge couplings, and  $\epsilon_{12} = -1$ .

The doublet fields  $H_1$  and  $H_2$  are decomposed in the following way:

$$\begin{aligned} H_1 &= \begin{pmatrix} H_1^1 \\ H_1^2 \end{pmatrix} = \begin{pmatrix} v_1 + (\phi_1^0 + i\chi_1^0)/\sqrt{2} \\ \phi_1^- \end{pmatrix}, \\ H_2 &= \begin{pmatrix} H_2^1 \\ H_2^2 \end{pmatrix} = \begin{pmatrix} \phi_2^+ \\ v_2 + (\phi_2^0 + i\chi_2^0)/\sqrt{2} \end{pmatrix}. \end{aligned} \quad (2)$$

The potential eq. (1) can be described with the help of two independent parameters (besides  $g, g'$ ):  $\tan \beta = v_2/v_1$  and  $M_A^2 = -m_{12}^2(\tan \beta + \cot \beta)$ , where  $M_A$  is the mass of the  $\mathcal{CP}$ -odd  $A$  boson.

In order to obtain the  $\mathcal{CP}$ -even neutral mass eigenstates, the rotation

$$\begin{pmatrix} H^0 \\ h^0 \end{pmatrix} = \begin{pmatrix} \cos \alpha & \sin \alpha \\ -\sin \alpha & \cos \alpha \end{pmatrix} \begin{pmatrix} \phi_1^0 \\ \phi_2^0 \end{pmatrix} \quad (3)$$

is performed, where the mixing angle  $\alpha$  is given in terms of  $\tan \beta$  and  $M_A$  by

$$\tan 2\alpha = \tan 2\beta \frac{M_A^2 + M_Z^2}{M_A^2 - M_Z^2}, \quad -\frac{\pi}{2} < \alpha < 0. \quad (4)$$

At tree level the mass matrix of the neutral  $\mathcal{CP}$ -even Higgs bosons is given in the  $\phi_1 - \phi_2$  basis in terms of  $M_Z$  and  $M_A$  by

$$\begin{aligned} M_{\text{Higgs}}^{2,\text{tree}} &= \begin{pmatrix} m_{\phi_1}^2 & m_{\phi_1 \phi_2}^2 \\ m_{\phi_1 \phi_2}^2 & m_{\phi_2}^2 \end{pmatrix} \\ &= \begin{pmatrix} M_A^2 \sin^2 \beta + M_Z^2 \cos^2 \beta & -(M_A^2 + M_Z^2) \sin \beta \cos \beta \\ -(M_A^2 + M_Z^2) \sin \beta \cos \beta & M_A^2 \cos^2 \beta + M_Z^2 \sin^2 \beta \end{pmatrix}, \end{aligned} \quad (5)$$

which then has to be rotated with the angle  $\alpha$  according to eq. (3), and one obtains the tree-level Higgs-boson masses

$$M_{\text{Higgs}}^{2,\text{tree}} \xrightarrow{\alpha} \begin{pmatrix} m_{H,\text{tree}}^2 & 0 \\ 0 & m_{h,\text{tree}}^2 \end{pmatrix}. \quad (6)$$

In the Feynman-diagrammatic approach the one-loop corrected Higgs masses are derived by finding the poles of the  $h - H$ -propagator matrix whose inverse is given by

$$(\Delta_{\text{Higgs}})^{-1} = -i \begin{pmatrix} q^2 - m_{H,\text{tree}}^2 + \hat{\Sigma}_H(q^2) & \hat{\Sigma}_{hH}(q^2) \\ \hat{\Sigma}_{hH}(q^2) & q^2 - m_{h,\text{tree}}^2 + \hat{\Sigma}_h(q^2) \end{pmatrix}, \quad (7)$$

where the  $\hat{\Sigma}$  denote the full one-loop contributions to the renormalized Higgs-boson self-energies. For these self-energies we take the result of the complete one-loop on-shell calculation of Ref. [5]. The agreement with the result obtained in Ref. [4] is better than 1 GeV for almost the whole MSSM parameter space.

As mentioned above the dominant contribution arises from the  $t - \tilde{t}$ -sector. The current eigenstates of the scalar quarks,  $\tilde{q}_L$  and  $\tilde{q}_R$ , mix to give the mass eigenstates  $\tilde{q}_1$  and  $\tilde{q}_2$ . The non-diagonal entry in the scalar quark mass matrix is proportional to the mass of the quark and reads for the  $\tilde{t}$ -mass matrix

$$m_t M_t^{LR} = m_t (A_t - \mu \cot \beta), \quad (8)$$

where we have adopted the conventions used in Ref. [17]. Due to the large value of  $m_t$  mixing effects have to be taken into account. Diagonalizing the  $\tilde{t}$ -mass matrix one obtains the eigenvalues  $m_{\tilde{t}_1}$  and  $m_{\tilde{t}_2}$  and the  $\tilde{t}$  mixing angle  $\theta_{\tilde{t}}$ .

The leading two-loop corrections have been obtained in Ref. [13] by calculating the  $\mathcal{O}(\alpha\alpha_s)$  contribution of the  $t - \tilde{t}$ -sector to the renormalized Higgs-boson self-energies at zero external momentum from the Yukawa part of the theory. Since this calculation was performed in the  $\phi_1 - \phi_2$ -basis, we perform the rotation into the  $h - H$ -basis according to eq. (3):

$$\begin{aligned} \hat{\Sigma}_H^{(2)} &= \cos^2 \alpha \hat{\Sigma}_{\phi_1}^{(2)} + \sin^2 \alpha \hat{\Sigma}_{\phi_2}^{(2)} + 2 \sin \alpha \cos \alpha \hat{\Sigma}_{\phi_1 \phi_2}^{(2)} \\ \hat{\Sigma}_h^{(2)} &= \sin^2 \alpha \hat{\Sigma}_{\phi_1}^{(2)} + \cos^2 \alpha \hat{\Sigma}_{\phi_2}^{(2)} - 2 \sin \alpha \cos \alpha \hat{\Sigma}_{\phi_1 \phi_2}^{(2)} \\ \hat{\Sigma}_{hH}^{(2)} &= -\sin \alpha \cos \alpha (\hat{\Sigma}_{\phi_1}^{(2)} - \hat{\Sigma}_{\phi_2}^{(2)}) + (\cos^2 \alpha - \sin^2 \alpha) \hat{\Sigma}_{\phi_1 \phi_2}^{(2)}. \end{aligned} \quad (9)$$

At the two-loop level the matrix (7) then consists of the renormalized Higgs-boson self-energies

$$\hat{\Sigma}_s(q^2) = \hat{\Sigma}_s^{(1)}(q^2) + \hat{\Sigma}_s^{(2)}(0), \quad s = h, H, hH, \quad (10)$$

where the momentum dependence is neglected only in the two-loop contribution. The Higgs-boson masses at the two-loop level are obtained by determining the poles of the matrix  $\Delta_{\text{Higgs}}$  in eq. (7).

We have implemented two further steps of refinement into the prediction for  $m_h$ , which are shown separately in the plots below. The leading two-loop Yukawa correction of  $\mathcal{O}(G_F^2 m_t^6)$  is taken over from the result obtained by renormalization group methods. It reads [8, 14]

$$\Delta m_h^2 = \frac{9}{16\pi^4} G_F^2 m_t^6 [\tilde{X}t + t^2] \quad (11)$$

$$\begin{aligned} \text{with } \tilde{X} &= \left[ \left( \frac{m_{\tilde{t}_2}^2 - m_{\tilde{t}_1}^2}{4m_t^2} \sin^2 2\theta_{\tilde{t}} \right)^2 \left( 2 - \frac{m_{\tilde{t}_2}^2 + m_{\tilde{t}_1}^2}{m_{\tilde{t}_2}^2 - m_{\tilde{t}_1}^2} \log \left( \frac{m_{\tilde{t}_2}^2}{m_{\tilde{t}_1}^2} \right) \right) \right. \\ &\quad \left. + \frac{m_{\tilde{t}_2}^2 - m_{\tilde{t}_1}^2}{2m_t^2} \sin^2 2\theta_{\tilde{t}} \log \left( \frac{m_{\tilde{t}_2}^2}{m_{\tilde{t}_1}^2} \right) \right], \end{aligned} \quad (12)$$

$$t = \frac{1}{2} \log \left( \frac{m_{\tilde{t}_1}^2 m_{\tilde{t}_2}^2}{m_t^4} \right). \quad (13)$$

The second step of refinement concerns leading QCD corrections beyond two-loop order, taken into account by using the  $\overline{MS}$  top mass,  $\overline{m}_t = \overline{m}_t(m_t) \approx 166.5$  GeV, for the two-loop contributions instead of the pole mass,  $m_t = 175$  GeV. In the  $\tilde{t}$  mass matrix, however, we continue to use the pole mass as an input parameter. Only when performing the comparison with the RG results we use  $\overline{m}_t$  in the  $\tilde{t}$  mass matrix for the two-loop result, since in the RG results the running masses appear everywhere. This three-loop effect gives rise to a shift up to 1.5 GeV in the prediction for  $m_h$ .

For the numerical evaluation we have chosen two values for  $\tan\beta$  which are favored by SUSY-GUT scenarios [18]:  $\tan\beta = 1.6$  for the  $SU(5)$  scenario and  $\tan\beta = 40$  for the  $SO(10)$  scenario. Other parameters are  $M_Z = 91.187$  GeV,  $M_W = 80.375$  GeV,  $G_F = 1.16639 \cdot 10^{-5}$  GeV<sup>-2</sup>,  $\alpha_s(m_t) = 0.1095$ , and  $m_t = 175$  GeV. For the figures below we have furthermore chosen  $M = 400$  GeV ( $M$  is the soft SUSY breaking parameter in the chargino and neutralino sector),  $M_A = 500$  GeV, and  $m_{\tilde{g}} = 500$  GeV as typical values (if not indicated differently). The scalar top masses and the mixing angle are derived from the parameters  $M_{\tilde{t}_L}$ ,  $M_{\tilde{t}_R}$  and  $M_t^{LR}$  of the  $\tilde{t}$  mass matrix (our conventions are the same as in Ref. [17]). In the figures below we have chosen  $m_{\tilde{q}} \equiv M_{\tilde{t}_L} = M_{\tilde{t}_R}$ .

The plot in Fig. 1 shows the result for  $m_h$  obtained from the diagrammatic calculation of the full one-loop and leading two-loop contributions. The two steps of refinement discussed above are shown in separate curves. For comparison the pure one-loop result is also given. The results are plotted as a function of  $M_t^{LR}/m_{\tilde{q}}$ , where  $m_{\tilde{q}}$  is fixed to 500 GeV. The qualitative behavior is the same as in Ref. [13], where the result containing only the leading one-loop contribution (and without further refinements) was shown. The two-loop contributions give rise to a large reduction of the one-loop result of 10–20 GeV. The two steps of refinement both increase  $m_h$  by up to 2 GeV. A minimum occurs for  $M_t^{LR} = 0$  GeV which we refer to as ‘no mixing’. A maximum in the two-loop result for  $m_h$  is reached for about  $M_t^{LR}/m_{\tilde{q}} \approx 2$  in the  $\tan\beta = 1.6$  scenario as well as in the  $\tan\beta = 40$  scenario. This case we refer to as ‘maximal mixing’. The maximum is shifted compared to its one-loop value of about  $M_t^{LR}/m_{\tilde{q}} \approx 2.4$ . The two steps of refinement have only a negligible effect on the location of the maximum.

In Fig. 2  $m_h$  is shown in the two scenarios with  $\tan\beta = 1.6$  and  $\tan\beta = 40$  as a function of  $m_{\tilde{q}}$  for no mixing and maximal mixing. The tree-level, the one-loop and the two-loop results with the two steps of refinement are shown (the values of  $m_{\tilde{q}}$  are such that the corresponding  $\tilde{t}$ -masses lie within the experimentally allowed region). In all scenarios of Fig. 2 the two-loop corrections give rise to a large reduction of the one-loop value of  $m_h$ . The biggest effect occurs for the  $\tan\beta = 1.6$  scenario with maximal mixing. The inclusion of the refinement terms leads to a slight shift in  $m_h$  towards higher values, whose size is about 20% of the two-loop correction. In the  $\tan\beta = 1.6$  scenario,  $m_h$  reaches about 80 GeV for  $m_{\tilde{q}} = 1$  TeV in the no-mixing case, and about 100 GeV for  $m_{\tilde{q}} = 1$  TeV in the maximal-mixing case. For  $\tan\beta = 40$  the respective values of  $m_h$  are nearly 115 GeV in the no-mixing case, and almost 130 GeV in the maximal-mixing case.

Varying the gaugino parameter  $M$ , which enters via the non-leading one-loop contributions, in the results of Fig. 2 changes the value of  $m_h$  within 3 GeV. Different values of the gluino mass,  $m_{\tilde{g}}$ , in the two-loop contribution affect the prediction for  $m_h$  by up to 3 GeV.

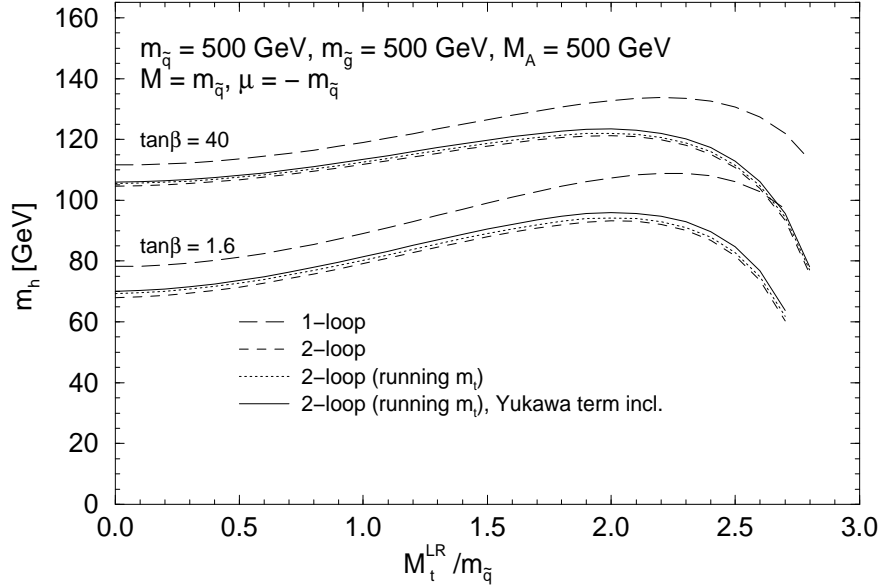


Figure 1: One- and two-loop results for  $m_h$  as a function of  $M_t^{LR}/m_{\tilde{q}}$  for two values of  $\tan\beta$ . The two steps of refinement discussed in the text are shown separately.

Allowing for a splitting between the parameters  $M_{\tilde{t}_L}$ ,  $M_{\tilde{t}_R}$  in the  $\tilde{t}$  mass matrix yields maximal values of  $m_h$  which are approximately the same as for the case  $m_{\tilde{q}} = M_{\tilde{t}_L} = M_{\tilde{t}_R}$  (see also Fig. 5 below). Varying  $\tan\beta$  around the value  $\tan\beta = 1.6$  leads to a relatively large effect in  $m_h$  (higher values for  $m_h$  are obtained for larger  $\tan\beta$ ), while the effect of varying  $\tan\beta$  around  $\tan\beta = 40$  is marginal. A more detailed analysis of the dependence of our results on the different SUSY parameters will be presented in a forthcoming publication. The discovery limit of LEP2 is expected to be slightly above 100 GeV [15]. Accordingly, our results confirm that for the scenario with  $\tan\beta = 1.6$  practically the whole parameter space of the MSSM can be covered at LEP2. For slightly larger  $\tan\beta$  and maximal mixing, however, some parameter space could remain in which the Higgs boson escapes detection at LEP2. For  $\tan\beta = 40$ , on the other hand, a full exploration of the MSSM parameter space will not be possible at LEP2. While the prediction for  $m_h$  is at the edge of the LEP2 range in the no-mixing case, the case of large mixing will be a challenge for the upgraded Tevatron or will finally be probed at LHC.

We now turn to the comparison of our diagrammatic results with the predictions obtained via renormalization group methods. We begin with the case of vanishing mixing in the  $\tilde{t}$  sector and large values of  $M_A$ , for which the RG approach is most easily applicable and is expected to work most accurately. In order to study different contributions separately, we have first compared the diagrammatic one-loop on-shell result [5] with the one-loop leading log result (without renormalization group improvement) given in Ref. [10] and found very good agreement, typically within 1 GeV. We then performed a leading log expansion of our

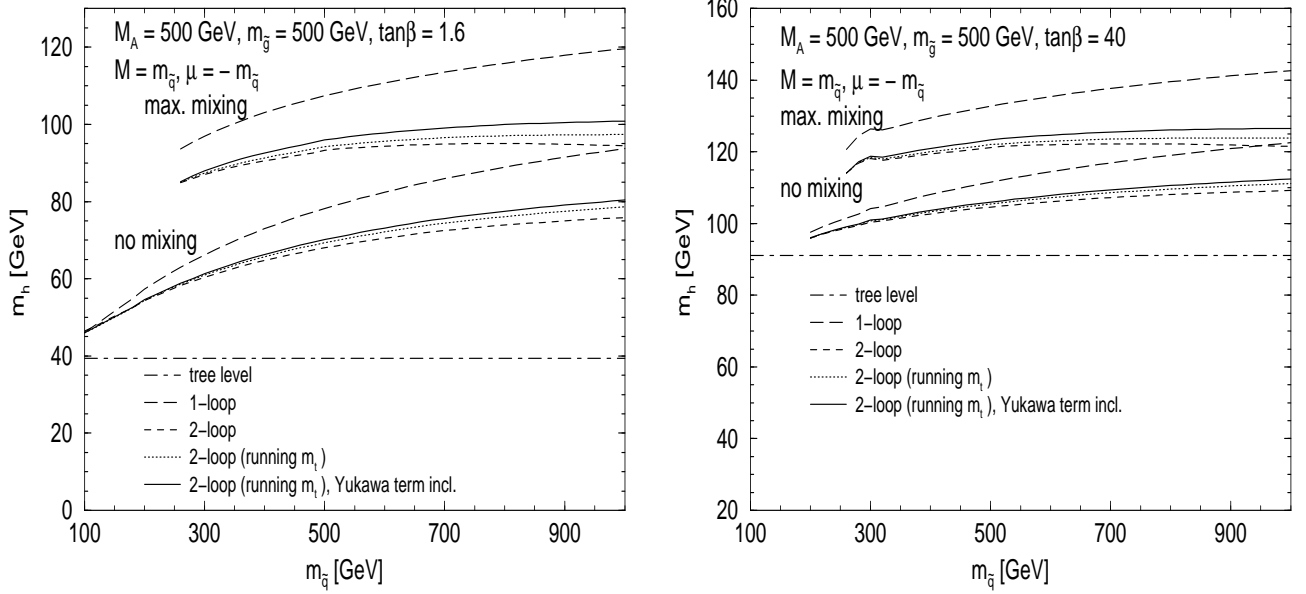


Figure 2: The mass of the lightest Higgs boson for  $\tan \beta = 1.6$  and  $\tan \beta = 40$ . The tree-level, the one-loop and the two-loop results for  $m_h$  are shown as a function of  $m_{\tilde{g}}$  for the no-mixing and the maximal-mixing case.

diagrammatic result (which corresponds to the two-loop contribution in the RG approach) and also found agreement with the full two-loop result within about 1 GeV. Finally, as shown in Fig. 3, we have compared our diagrammatic result for the no-mixing case including the refinement terms with the RG results obtained in Ref. [9].<sup>1</sup> As can be seen in Fig. 3, after the inclusion of the refinement terms the diagrammatic result for the no-mixing case agrees very well with the RG result. The deviation between the results exceeds 2 GeV only for  $\tan \beta = 1.6$  and  $m_{\tilde{g}} < 150$  GeV. For smaller values of  $M_A$  the comparison for the no-mixing case looks qualitatively the same. For  $\tan \beta = 1.6$  and values of  $M_A$  below 100 GeV slightly larger deviations are possible. Since the RG results do not contain the gluino mass as a parameter, varying  $m_{\tilde{g}}$  gives rise to an extra deviation, which in the no-mixing case does not exceed 1 GeV. Varying the other parameters  $\mu$  and  $M$  in general does not lead to a sizable effect in the comparison with the corresponding RG results.

We now consider the situation when mixing in the  $\tilde{t}$  sector is taken into account. We have again compared the full one-loop result with the one-loop leading log result used within the RG approach [10] and found good agreement. Only for values of  $M_A$  below 100 GeV and large mixing deviations of about 5 GeV occur. In Fig. 4 our diagrammatic result including the refinement terms is compared with the RG results [9] as a function of  $M_t^{LR}/m_{\tilde{g}}$  for  $\tan \beta = 1.6$  and  $\tan \beta = 40$ . The point  $M_t^{LR}/m_{\tilde{g}} = 0$  corresponds to the plots shown in Fig. 3, except that the parameter  $\mu$  is now set to  $\mu = -m_{\tilde{g}}$ . For larger  $\tilde{t}$ -mixing sizable

<sup>1</sup>The RG results of Ref. [9] and Ref. [10] agree within about 2 GeV with each other.

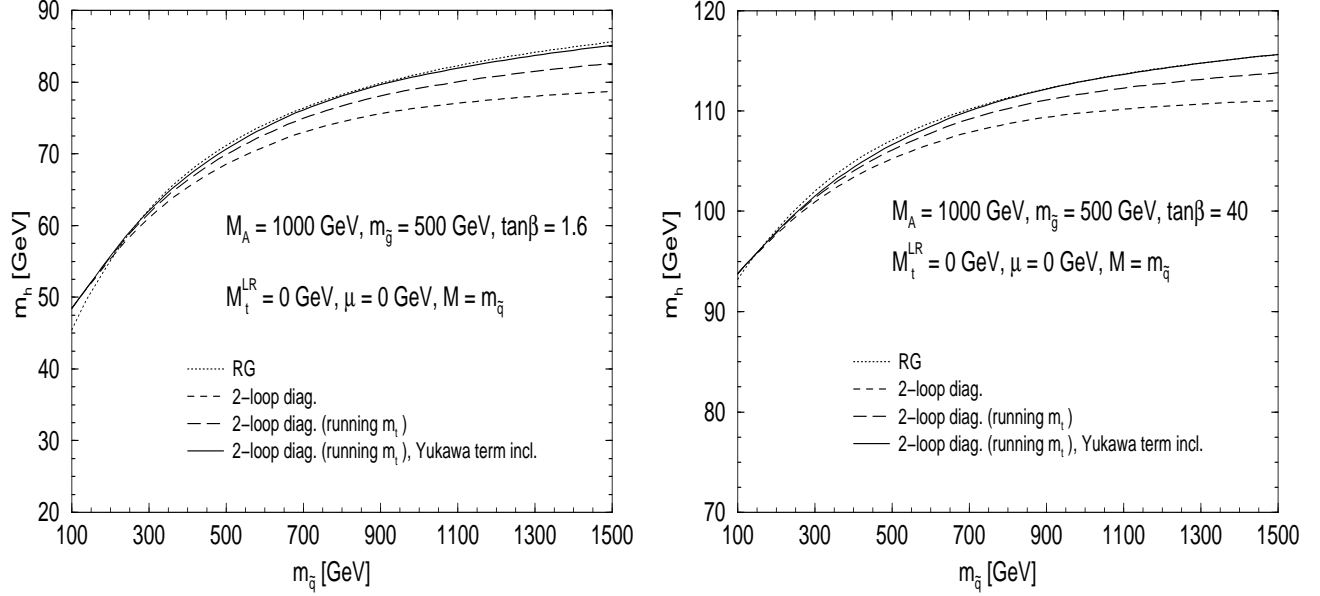


Figure 3: Comparison between the Feynman-diagrammatic calculations and the results obtained by renormalization group methods [9]. The mass of the lightest Higgs boson is shown for the two scenarios with  $\tan\beta = 1.6$  and  $\tan\beta = 40$  for the case of vanishing mixing in the  $\tilde{t}$ -sector.

deviations between the diagrammatic and the RG results occur, which can exceed 5 GeV for moderate mixing and become very large for large values of  $M_t^{LR}/m_{\tilde{g}}$ . As already stressed above, the maximal value for  $m_h$  in the diagrammatic approach is reached for  $M_t^{LR}/m_{\tilde{g}} \approx 2$ , whereas the RG results have a maximum at  $M_t^{LR}/m_{\tilde{g}} \approx 2.4$ , i.e. at the one-loop value. Varying the value of  $m_{\tilde{g}}$  in our result leads to a larger effect than in the no-mixing case and shifts the diagrammatic result relative to the RG result within  $\pm 2$  GeV.

The results of our diagrammatic on-shell calculation and the RG methods have been compared above in terms of the parameters  $M_{\tilde{t}_L}$ ,  $M_{\tilde{t}_R}$  and  $M_t^{LR}$  of the  $\tilde{t}$  mixing matrix, since the available numerical codes for the RG results [9, 10] are given in terms of these parameters. However, since the two approaches rely on different renormalization schemes, the meaning of these (non-observable) parameters is not precisely the same in the two approaches starting from two-loop order. Indeed we have checked that assuming fixed values for the physical parameters  $m_{\tilde{t}_1}$ ,  $m_{\tilde{t}_2}$ , and  $\theta_{\tilde{t}}$  and deriving the corresponding values of the parameters  $M_{\tilde{t}_L}$ ,  $M_{\tilde{t}_R}$  and  $M_t^{LR}$  in the on-shell scheme as well as in the  $\overline{MS}$  scheme, sizable differences occur between the values of the mixing parameter  $M_t^{LR}$  in the two schemes, while the parameters  $M_{\tilde{t}_L}$ ,  $M_{\tilde{t}_R}$  are approximately equal in the two schemes. Thus, part of the different shape of the curves in Fig. 4 may be attributed to a different meaning of the parameter  $M_t^{LR}$  in the on-shell scheme and in the RG calculation.

In order to compare results obtained by different approaches making use of different



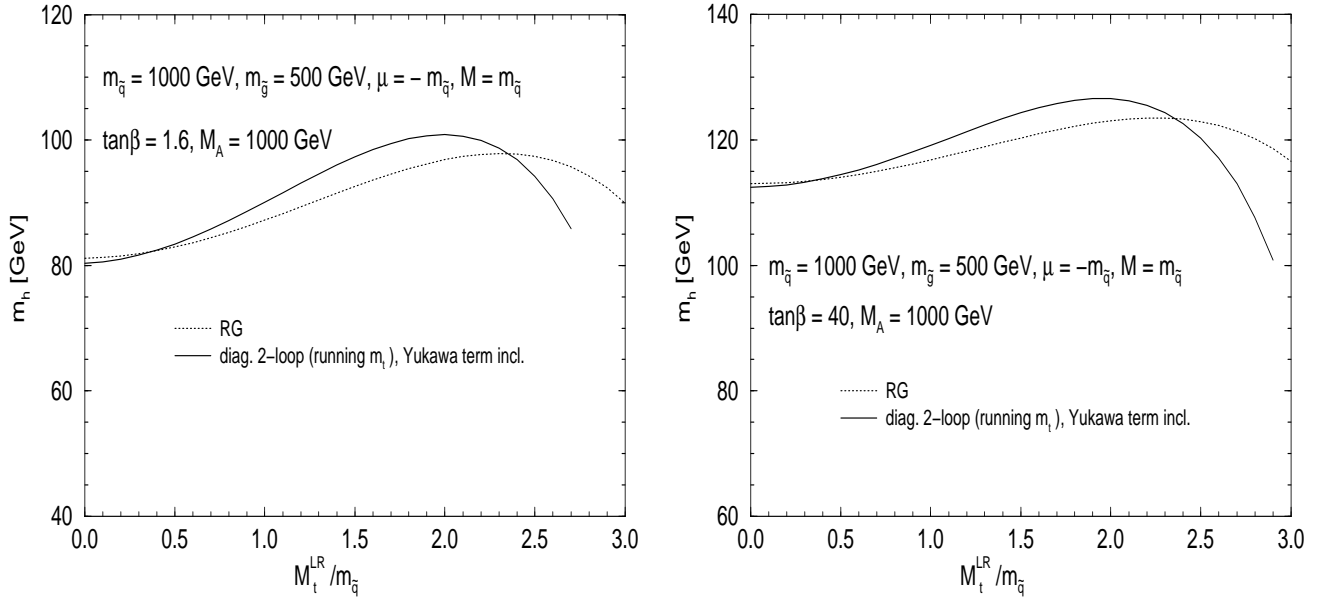


Figure 4: Comparison between the Feynman-diagrammatic calculations and the results obtained by renormalization group methods [9]. The mass of the lightest Higgs boson is shown for the two scenarios with  $\tan\beta = 1.6$  and  $\tan\beta = 40$  for increasing mixing in the  $\tilde{t}$ -sector and  $m_{\tilde{q}} = M_A$ .

renormalization schemes we find it preferable to compare predictions for physical observables in terms of other observables (instead of unphysical parameters). As a step into this direction we compare in Fig. 5 the diagrammatic results and the RG results as a function of the physical mass  $m_{\tilde{t}_2}$  and with the mass difference  $\Delta m_{\tilde{t}} = m_{\tilde{t}_2} - m_{\tilde{t}_1}$  and the mixing angle  $\theta_{\tilde{t}}$  as parameters. In the context of the RG approach the running  $\tilde{t}$  masses, derived from the  $\tilde{t}$  mass matrix, are considered as an approximation for the physical masses. The range of the  $\tilde{t}$  masses appearing in Fig. 5 has been constrained by requiring that the contribution of the third generation of scalar quarks to the  $\rho$ -parameter [17] does not exceed the value of  $1.3 \cdot 10^{-3}$ , which corresponds to the resolution of  $\Delta\rho (= \epsilon_1)$  when it is determined from experimental data [19]. As in the comparison performed above, in Fig. 5 very good agreement is found between the results of the two approaches in the case of vanishing  $\tilde{t}$  mixing. For the maximal mixing angle  $\theta_{\tilde{t}} = -\pi/4$ , however, the diagrammatic result yields values for  $m_h$  which are higher by about 5 GeV.

In summary, we have implemented the result of the Feynman-diagrammatic calculation of the leading  $\mathcal{O}(\alpha\alpha_s)$  corrections to the masses of the neutral  $\mathcal{CP}$ -even Higgs bosons in the MSSM into the prediction based on the complete diagrammatic one-loop on-shell result. Two further refinements have been added in order to incorporate leading electroweak two-loop and higher-order QCD contributions. In this way we provide the at present most precise

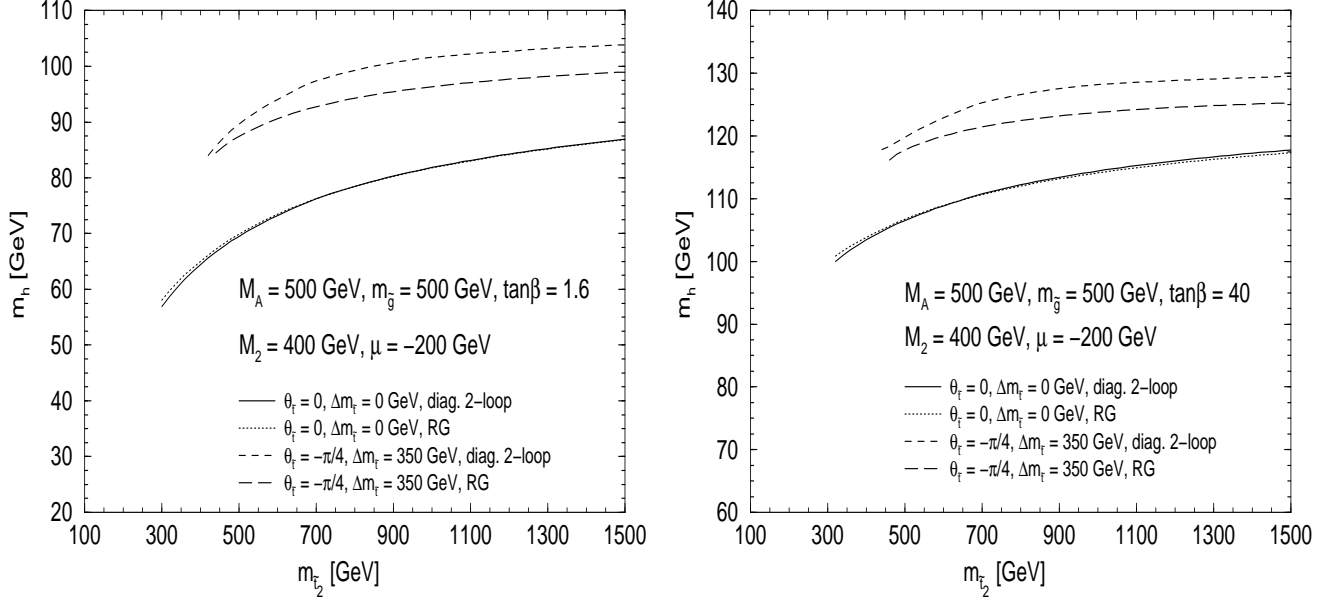


Figure 5: Comparison between the Feynman-diagrammatic calculations and the results obtained by renormalization group methods [9]. The mass of the lightest Higgs boson is shown for the two scenarios with  $\tan \beta = 1.6$  and  $\tan \beta = 40$  as a function of the heavier physical  $\tilde{t}$  mass  $m_{\tilde{t}_2}$ . For the curves with  $\theta_{\tilde{t}} = 0$  a mass difference  $\Delta m_{\tilde{t}} = 0$  GeV is assumed whereas for  $\theta_{\tilde{t}} = -\pi/4$  we chose  $\Delta m_{\tilde{t}} = 350$  GeV, for which the maximal Higgs masses are achieved.

prediction for  $m_h$  based on Feynman-diagrammatic results. The results are valid for arbitrary values of the relevant MSSM parameters. The two-loop corrections lead to a large reduction of the one-loop on-shell result. Concerning the discovery and exclusion potential of LEP2, our results confirm that the scenario with low  $\tan \beta$  ( $\tan \beta = 1.6$ ) in the MSSM should be covered at LEP2, while the scenario with high  $\tan \beta$  ( $\tan \beta = 40$ ) is only (partly) accessible for vanishing mixing in the scalar top sector. We have compared our results with the results obtained via RG methods, and have analyzed in this context the one-loop and two-loop contributions separately. We have found that the drastic deviations present between the one-loop on-shell result and the RG result are largely reduced. For the case of vanishing mixing in the scalar top sector the diagrammatic and the RG results agree very well, while sizable deviations exceeding 5 GeV occur when  $\tilde{t}$  mixing is taken into account. Since the gluino mass does not appear as a parameter in the RG results, its variation gives rise to an extra deviation which lies within  $\pm 2$  GeV. We have discussed the issue of how the results obtained via different approaches using different renormalization schemes can be formulated such that they are readily comparable to each other also when corrections beyond one-loop order are incorporated. For this purpose it is very desirable to express the prediction for the Higgs-boson masses in terms of physical observables, i.e. the physical masses and mixing

angles of the model.

We thank M. Carena, H. Haber and C. Wagner for fruitful discussions and communication about the numerical comparison of our results. We also thank A. Djouadi and M. Spira for helpful discussions.

## References

- [1] G. Kane, C. Kolda and J. Wells, *Phys. Rev. Lett.* **70** (1993) 2686;  
J. Espinosa and M. Quirós, *Phys. Lett.* **B 302** (1993) 51; *Phys. Rev. Lett.* **81** (1998) 516.
- [2] H. Haber and G. Kane, *Phys. Rep.* **117** (1985) 75.  
H.P. Nilles, *Phys. Rep.* **110** (1984) 1.
- [3] H. Haber and R. Hempfling, *Phys. Rev. Lett.* **66** (1991) 1815;  
Y. Okada, M. Yamaguchi and T. Yanagida, *Prog. Theor. Phys.* **85** (1991) 1;  
J. Ellis, G. Ridolfi and F. Zwirner, *Phys. Lett.* **B 257** (1991) 83; *Phys. Lett.* **B 262** (1991) 477;  
R. Barbieri and M. Frigeni, *Phys. Lett.* **B 258** (1991) 395.
- [4] P. Chankowski, S. Pokorski and J. Rosiek, *Nucl. Phys.* **B 423** (1994) 437.
- [5] A. Dabelstein, *Nucl. Phys.* **B 456** (1995) 25; *Z. Phys.* **C 67** (1995) 495.
- [6] J. Bagger, K. Matchev, D. Pierce and R. Zhang, *Nucl. Phys.* **B 491** (1997) 3.
- [7] J. Casas, J. Espinosa, M. Quirós and A. Riotto, *Nucl. Phys.* **B 436** (1995) 3, E: *ibid.* **B 439** (1995) 466.
- [8] M. Carena, J. Espinosa, M. Quirós and C. Wagner, *Phys. Lett.* **B 355** (1995) 209.
- [9] M. Carena, M. Quirós and C. Wagner, *Nucl. Phys.* **B 461** (1996) 407.
- [10] H. Haber, R. Hempfling and A. Hoang, *Z. Phys.* **C 75** (1997) 539.
- [11] R. Hempfling and A. Hoang, *Phys. Lett.* **B 331** (1994) 99.
- [12] *Reports of the Working Group on Precision Calculations for the Z-resonance*, CERN Yellow Report, CERN 95-03, eds. D. Bardin, W. Hollik and G. Passarino.
- [13] S. Heinemeyer, W. Hollik and G. Weiglein, KA-TP-2-1998, hep-ph/9803277, to appear in *Phys. Rev.* **D**.
- [14] M. Carena, P. Chankowski, S. Pokorski and C. Wagner, FERMILAB-PUB-98/146-T, hep-ph/9805349.

- [15] M. Carena and P. Zerwas, in *Physics at LEP2*, CERN 96-01, eds. G. Altarelli, T. Sjöstrand and F. Zwirner.
- [16] J. Gunion, H. Haber, G. Kane and S. Dawson, *The Higgs Hunter's Guide*, Addison-Wesley, 1990.
- [17] A. Djouadi, P. Gambino, S. Heinemeyer, W. Hollik, C. Jünger and G. Weiglein, *Phys. Rev. Lett.* **78** (1997) 3626; *Phys. Rev.* **D 57** (1998) 4179.
- [18] M. Carena, S. Pokorski and C. Wagner, *Nucl. Phys.* **B406** (1993) 59; W. de Boer et al., *Z. Phys.* **C 71** (1996) 415.
- [19] G. Altarelli, XVIII Int. Symposium on Lepton–Photon Interactions, Hamburg 1997, CERN-TH 97-278, hep-ph/9710434